Nguyen Van Phap[1,*], Nguyen Trac Toan[1], Vu Hong Quan[1], Nguyen Van Tuan[1], Dam The Hieu[1], Luong Minh Duc[1]

An Advanced Standalone GNSS Navigation Architecture for High-Dynamic Applications via Carrier Phase TDDD with Rapid Hotstart Capability

Journal of Electrical Systems

Abstract: - This research addresses the challenges of accuracy and reliability in Standalone Global Navigation Satellite System (GNSS) receivers under high dynamic (HD) applications, where signal loss-of-lock is frequent. An advanced architectural design is proposed, utilizing carrier phase measurements and the Time-Differenced Double Difference (TDDD) method. To ensure robust tracking, a 5-state Kalman Filter (KF)-based tracking loop replaces the traditional Phase-Locked Loop (PLL), optimizing phase, frequency, and frequency derivative to enhance sensitivity. The reliable phase data is processed by a 9-state TDDD Positioning KF (PKF), which features an extended model for estimating high-order acceleration components. Measurement quality is maintained using the Normalized Innovation Squared (NIS) test to effectively eliminate cycle slips. The Sequential Kalman Filter (SKF) is employed to simplify implementation and ensure realtime capability. Significantly, the architecture incorporates a rapid hotstart mechanism to minimize the Time To First Fix (TTFF), ensuring the agility required for HD maneuvers. The entire proposed architecture was *successfully* implemented and validated on the Field-Programmable Gate Array (FPGA) Zynq-7000 platform, confirming its efficiency and suitability for realtime HD GNSS processing. The model significantly improves positioning performance compared to traditional methods, providing a robust solution for independent GNSS navigation.

Keywords*:* Time-differenced double difference method, Standalone GNSS, Sequential Kalman filter, Hotstart, Zynq-7000.

I INTRODUCTION

In positioning applications for HD platforms, such as missiles or hypersonic aircraft with velocities exceeding Mach 5 and extreme acceleration, navigation systems typically integrate data from a GNSS receiver and an Inertial Navigation System (INS) [1]. While the INS assists the GNSS receiver by predicting signal phase and Doppler frequency to bridge short-term outages, its inherent drift error accumulates over time, potentially leading to system divergence [2]. Consequently, the GNSS receiver must maintain robust autonomous operation to independently re-acquire signals and recover its navigation state if the INS becomes unreliable.

Crucially, in such HD maneuvers, a rapid hotstart capability is not merely an enhancement but a fundamental requirement. Minimizing the Time To First Fix (TTFF) ensures that the receiver can achieve a near instantaneous transition from signal re-acquisition to a full navigation solution [3]. This rapid recovery is vital to prevent catastrophic navigation failure during critical flight phases, where even a few seconds of 'blind' flight due to signal loss-of-lock can result in significant trajectory deviations. Therefore, a high performance standalone GNSS architecture must provide not only high accuracy and high frequency updates but also a resilient hotstart mechanism to ensure continuous mission integrity.

To overcome these limitations, this paper proposes an advanced standalone architecture featuring a Rapid Hotstart mechanism designed specifically for HD applications. Unlike traditional methods, our approach achieves a minimal TTFF by proactively injecting three fundamental parameters: updated ephemeris, approximate user position, and precise time references. This integration allows the receiver to precalculate the visible satellite constellation and drastically narrow the Doppler search space, shifting from a global search to a targeted acquisition strategy. By streamlining this process on the Zynq-7000 FPGA platform, the architecture ensures that the KF-based tracking loops can reestablish lock almost instantaneously, maintaining continuous navigation integrity even after severe signal disruptions.

One of the recent research directions aimed at enhancing the accuracy of GNSS receivers is the use of the TDDD method. This approach exploits the differences in GNSS measurements over time and across satellites to eliminate clock errors, atmospheric delays caused by the ionosphere, and systemic noise. TDDD is particularly useful in HD conditions because low-frequency biases can be suppressed through temporal differentiation, while retaining the necessary phase and code information for accurate relative positioning. Numerous studies have shown that TDDD significantly improves positioning quality [4-12].

[1] Viettel Aerospace Institute, Ha Noi, 100000, Viet Nam
*Corresponding author: phapnv@viettel.com.vn

To sustain the signal tracking loop under HD conditions, the authors of [4-6] utilized an INS, which can account for rapid motion or swift maneuvers. The authors in [7] developed multi-GNSS Precise Point Positioning (PPP) by combining Time-Differenced Double Difference (TDDD) measurements with non-differenced measurements. By employing time-differencing, this paper reduces several time constant parameters such as ambiguity, hardware biases, and other near static systematic errors. In [8], when motion is fast or complex, relying solely on Time-Differenced Carrier Phase (TDCP) or Doppler measurements may be limited they combined these two measurement types and utilized a factor graph optimization to enhance velocity reliability. Research [9] investigated the impact of the sampling rate on TDCP. They experimented with higher sampling rates for HD platforms (e.g., UAVs). If your definition of HD aligns with UAVs, aircraft, or fast moving devices, this paper is highly relevant, demonstrating the use of TDCP plus high sampling rates to capture rapid movements. However, the aforementioned authors have not thoroughly or fully addressed the problem of ensuring positioning quality for a Standalone GNSS receiver operating robustly under extreme HD conditions.

A crucial limitation of code measurements in the TDDD method is that the measurement noise is often not white noise but exhibits temporal correlation, particularly in environments strongly influenced by the ionosphere, troposphere, and clock jitter. This correlation reduces the efficiency of linear filters, such as the Kalman filter. Conversely, carrier phase measurements have smaller noise and are nearly temporally uncorrelated (white noise), as indicated in the study by Prochniewicz et al. [13]. Therefore, in applications demanding high accuracy and processing capability in HD environments, using the carrier phase instead of the code helps to improve data quality and the effectiveness of estimation filters.

Consequently, to enhance the positioning quality of a Standalone GNSS receiver in HD conditions, it is essential to first ensure the signal tracking loop can robustly acquire and track the signal under high dynamics, thereby providing reliable phase information. Based on the output of the tracking loop, a TDDD state model must be constructed which, beyond position and velocity, is capable of estimating high order dynamic components, such as acceleration.

In this paper, the signal tracking loop utilizes a 5-State Kalman filter, including: code phase error, carrier phase error, carrier Doppler error, carrier Doppler rate error, and carrier Doppler rate rate error. The estimated states are used to provide input information for the Numerically Controlled Oscillators (NCO) implemented on the FPGA, specifically updating frequency and phase. The tracking loop also receives supporting information at a lower frequency from the obtained positioning solution. During GNSS signal tracking under HD conditions, rapid changes in velocity and acceleration cause strong variations in Doppler and Doppler rate, leading to large frequency and phase errors. When using a traditional PLL, the loop bandwidth often has to be widened to cope with these rapid signal changes. However, widening the bandwidth increases measurement noise, thus degrading the accuracy of the phase estimate. Furthermore, the PLL only adjusts the NCO frequency without directly optimizing both phase and frequency simultaneously. To overcome these limitations, the Kalman filter is used as a replacement for the PLL in the signal tracking process. Unlike the PLL, the Kalman filter does not require a fixed feedback loop structure but performs an optimal estimation of phase, frequency, and frequency derivative states based on the signal's dynamic and noise models. Besides its ability to update weights over time, the Kalman filter can simultaneously correct both the NCO phase and frequency, helping to maintain high accuracy and stable tracking capability during rapid signal variation. Subsequently, the high accuracy information from the tracking loop is used to feed the TDDD positioning module, which utilizes a 9-State Kalman Filter encompassing position, velocity, and acceleration errors. The high precision information from the tracking loop enables the positioning loop to estimate navigation data with superior accuracy. When utilizing carrier phase measurements, the system is susceptible to cycle slips during sudden changes. Therefore, this paper develops a state and measurement model for phase in an independent form, rather than a cumulative measurement. Specifically, information regarding the phase change between time steps is determined and provided by the FPGA. The TDDD measurements are prechecked by the NIS method to eliminate outliers. NIS uses the measurement innovation information to evaluate whether the filter is operating 'consistently' with reality before the measurement is used, thereby minimizing the use of unreliable measurements and offering advantages over methods that rely on residuals. Finally, TDDD requires combining GNSS signals from observed satellites, which can result in a large computational load, potentially challenging realtime positioning implementation. In this paper, we propose implementing a SKF, processing measurements one satellite at a time. The SKF has been proven to yield results equivalent to a full state filter implementation but with significantly simpler deployment [14].

II SYSTEM MODEL

In this paper, the satellite navigation receiver is referred to as VT-GNSS. For GNSS receivers operating in HD applications integrated with an INS it is crucial to provide navigation data as early as possible to prevent INS drift. The VT-GNSS receiver achieves this by supplying coarse information, including the approximate position , approximate time, and ephemeris. Based on this data, the VT-GNSS can identify currently visible satellites, narrow the frequency domain search space, and provide early ephemeris information, thereby significantly reducing the Time To First Fix (TTFF). The operational principle of the hot-start process for the VT-GNSS receiver is illustrated in Fig. 1.

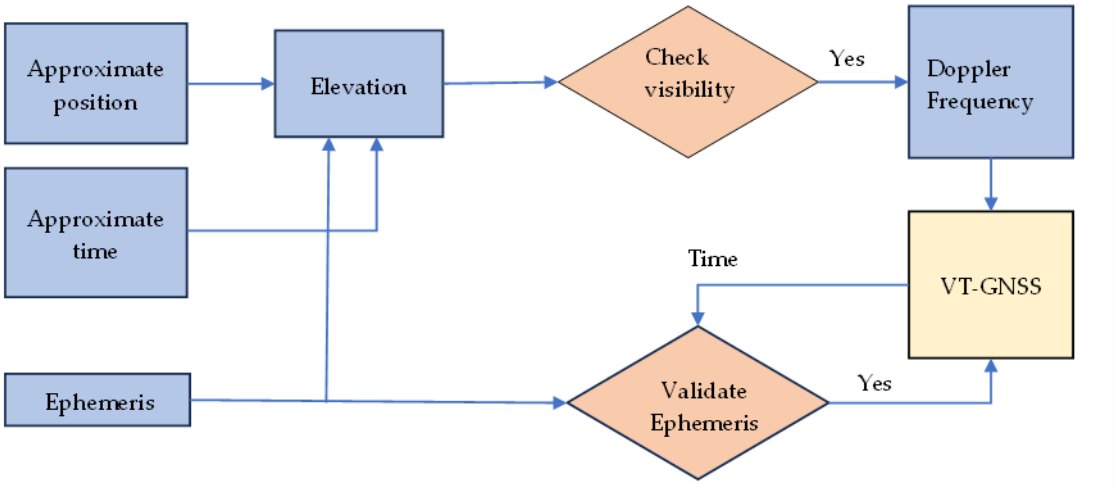

Figure 1 Hotstart for VT-GNSS

Based on the input parameters, the elevation angle of each satellite is determined to evaluate satellite visibility [3]. For every visible satellite, the corresponding Doppler frequency is calculated and fed into the VT-GNSS receiver. This mechanism effectively narrows the Doppler search space from 30000 Hz to less than 1000 Hz. Additionally, the Ephemeris information undergoes a validity check by comparing its timestamp with the reference time provided by the VT-GNSS (typically available after 6 seconds of operation). If the ephemeris is confirmed to be valid, it is immediately utilized for the navigation solution, ensuring a rapid and robust transition to full positioning mode.

To realize the TDDD method, the VT-GNSS receiver is implemented on the AMD Zynq 7000 SoC (System-on-Chip) platform via the MicroZed board. This architecture provides a unique synergy by integrating a Processing System (PS) and Programmable Logic (PL) on a single silicon die. The PS, featuring dual high performance Arm Cortex-A9 cores, manages software defined tasks and high level navigation algorithms, while the FPGA-based PL handles hardware level digital signal processing (DSP) and communicates with the PS through a high speed AXI bus [15]. By leveraging this hybrid structure, the VT-GNSS receiver effectively fulfills the rigorous requirements for flexibility, realtime computation, and the high speed processing necessary for tracking signals in HD environments.

The implementation strategy involves two main tasks: first, building dedicated IP Cores (such as CARRIER & CODE NCO and MULTI-CORRELATOR) on the PL to perform high speed data processing from the Front-End (up to tens of MHz), subsequently down sampling the results to KHz for the PS; and second, developing embedded software on the PS to execute complex tracking loops and positioning algorithms, which calculate position, velocity, and navigation parameters. This strategic division of labor maximizes the speed of the FPGA for realtime measurements while retaining software flexibility for implementing sophisticated positioning and signal filtering techniques. Figure 2 illustrates the TDDD principle diagram as implemented on Zynq 7000. In this paper, the receiver implementing the architecture shown in Figure 2 is referred to as VT-GNSS.

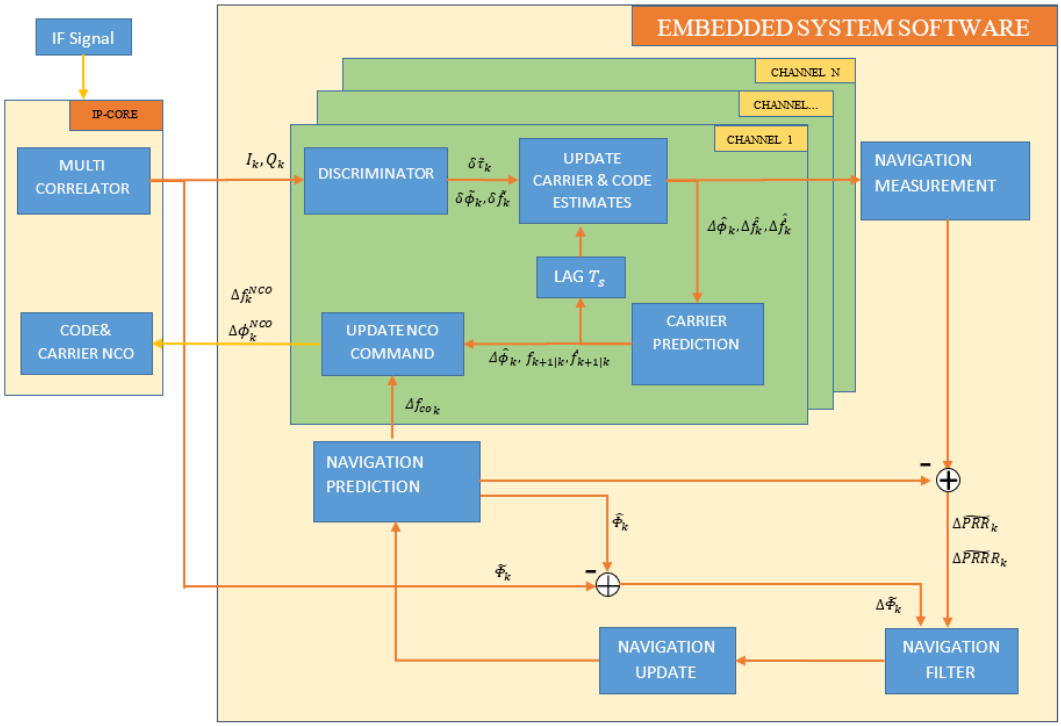

Figure 2 TDDD principle diagram

The accumulated value at step k, provided by the MULTI-CORRELATOR based on the received GNSS signal and the reference signal from the NCO, is supplied to the tracking loops on N channels corresponding to each observed satellite. Within each channel, the system evaluates errors in phase, Doppler frequency, Doppler rate, and Doppler rate rate, and forwards this information to the navigation block. This block determines the pseudorange rate (PRR) and pseudorange rate rate (PRRR) values in the NAVIGATION MEASUREMENT module and feeds them back to the NCO for reference signal correction in the next step. These measurement insights are then provided to the NAVIGATION FILTER, where the TDDD method is applied to determine navigation information such as position, velocity, and acceleration. The determined navigation data is subsequently used to predict the values of carrier phase, PRR, and PRRR in the NAVIGATION PREDICTION module for use in the NAVIGATION FILTER at step k+1. Finally, the navigation information provides updates to the NCO, thus forming a closed-loop system. Detailed signal processing is described in sections 2.1 and 2.2

2.1 GNSS Signal Tracking Loop Design

Under HD conditions, the GNSS signal is severely affected by variations in Doppler and its derivatives, leading to a sharp increase in phase and frequency errors. When using a traditional PLL, tracking the signal requires widening the PLL loop bandwidth [16]. However, this increases measurement noise and reduces phase accuracy. Furthermore, the PLL can only provide information to correct the NCO frequency, and errors in phase determination can also cause errors in Doppler frequency determination, subsequently introducing errors into the velocity estimate.

Using the Kalman Filter to maintain the signal tracking loop allows for the simultaneous and optimal estimation of phase, frequency, and frequency derivative based on the signal's dynamic model. Thanks to its ability to adaptively update weights over time, the Kalman filter not only maintains stable signal lock but also provides information for correcting both the NCO phase and frequency, thereby reducing errors and improving the accuracy of the signal tracking loop when the receiver operates under HD conditions.

In this paper, the signal tracking loop employs a non-coherent prefilter (NPF) form with 5 states, including: code phase error, carrier phase error, carrier Doppler error, carrier Doppler rate error and carrier Doppler rate rate error. The measurements used are the outputs of the Discriminators. The nonlinear error state space model in discrete form is utilized as follows:

$$x_{k+1} = f(x_k) + w_k, \qquad x_k \in R^5 \tag{1}$$

$$y_k = h(x_k) + v_k \tag{2}$$

The state error vector x_{k+1} is defined as:

$$x_{k+1} = \left[\Delta\tau_k \quad \Delta\phi_k \quad \Delta f_k \quad \Delta\dot{f}_k \quad \Delta\ddot{f}_k\right]^T \tag{3}$$

Where $f(\cdot)$ is the nonlinear dynamic function describing the state transition process, $h(\cdot)$ is the nonlinear function mapping the state to the measurement space, w_k, v_k are the process noise and measurement noise satisfy the following condition: $w_k, \sim\mathcal{N}(0,Q), v_k, \sim\mathcal{N}(0,R)$; $Q \in \mathcal{R}^{5\times5}$ is the process noise covariance matrix, $R \in \mathcal{R}^{3\times3}$ is the measurement noise covariance matrix; $\Delta\tau_k$: is the code phase error – chips (change to code period, second); $\Delta\phi_k$ is the carrier phase error – radian/2π (cycles); Δf_k is the carrier Doppler error, Hz; $\Delta\dot{f}_k$ is the carrier Doppler error rate, Hz/s; $\Delta\ddot{f}_k$ is the carrier Doppler error rate rate, Hz/S^2. In this paper, the symbol (^) describes the estimated value, (~) describes the measured value, and the index form k+1|k describes the predicted value at step k.

To apply the Extended Kalman Filter (EKF), the model is linearized around the estimated point $\hat{x}_{k|k}$. The approximated linear model is then expressed as follows:

$$\Delta x_{k+1} = \Phi_k \Delta x_k + w_k \tag{4}$$

$$\Delta z_k = H_k \Delta x_k + v_k \tag{5}$$

Where $\Phi_k = \left.\frac{\partial f}{\partial x}\right|_{x=\hat{x}_{k|k}}$ is the state transition matrix, $H_k = \left.\frac{\partial h}{\partial x}\right|_{x=\hat{x}_{k|k}}$ is the measurement matrix;

The state matrix is determined as follows:

$$\Phi_k = \begin{bmatrix} 1 & 0 & \beta T_s & \beta {T_s}^2/2 & \beta {T_s}^3/6 \\ 0 & 1 & T_s & {T_s}^2 & {T_s}^2/6 \\ 0 & 0 & 1 & T_s & {T_s}^2/2 \\ 0 & 0 & 0 & 1 & T_s \\ 0 & 0 & 0 & 0 & 1 \end{bmatrix} \tag{6}$$

Where T_s is the sample time, sec; $\beta = 1/F_{carrier}$; $F_{carrier}$ is the carrier frequency

The measurement matrix uses the output of the discriminators at step k as follows:

$$\begin{aligned} \delta\tilde{\tau}_k &= \Delta\tau_k + \frac{\beta T_s}{2}\Delta f_k + \frac{\beta T_s^2}{6}\Delta\dot{f}_k \\ \delta\tilde{\phi}_k &= \Delta\phi_k + T_s\Delta f_k + \frac{T_a^2}{3}\Delta\dot{f}_k \end{aligned} \tag{8}$$

The measurement matrix H_k is then determined as follows:

$$H_k = \begin{bmatrix} 1 & 0 & \frac{\beta T_s}{2} & \frac{\beta T_s^2}{6} & 0 \\ 0 & 1 & T_s & \frac{T_a^2}{3} & 0 \end{bmatrix} \tag{9}$$

The corresponding covariance matrix Q_k, R_k of the system model and measurement is determined as follows:

$$Q_k = E[w_k, w_k^T],\ R_k = E[v_k, v_k^T], \tag{10}$$

The detailed description of the components of matrix Q_k, R_k can be found in [17].

After linearizing the state model and measurement model using the Jacobians, the EKF operates in two steps. In the prediction step, the filter utilizes the linearized state model to predict the next state and propagates the error covariance matrix, which is performed in the CARRIER PREDICTION block. Subsequently, in the update step, the filter uses the linearized measurement model to correct the predicted state with the new measurement, while simultaneously updating the covariance matrix. Upon completing the update step, the final estimated state and estimated error for the current time are obtained in the UPDATE CARRIER & CODE ESTIMATES block. This information is then used to provide input to the UPDATE NCO COMMAND block/module to determine the frequency and phase required for the NCO.

$$\begin{aligned} \Delta {f_{ca}^{NCO}}_k &= f_{k+1|k} - F_0;\ \Delta {f_{co}^{NCO}}_k = F_{code}\left(1 + \frac{f_{k+1|k}}{F_{carrier}}\right) \\ \Delta {\phi_{ca}^{NCO}}_k &= \Delta\hat{\phi}_k;\ \Delta {\tau_{co}^{NCO}}_k = \Delta\hat{\tau}_k \end{aligned} \tag{11}$$

Where τ defines the filter update interval, F_0 is the initial frequency value of the NCO, and F_{code} is the code frequency (1.023 MHz for the GPS L1CA signal). In addition to updating the NCO with high frequency in the tracking block, the NCO frequency can also be corrected using the frequency from the navigation block based on the navigation results, determining the value $\Delta {f_{co}}_k$, detailed in [18].

2.2 Navigation Solution

The TDDD state model at step k used in this paper employs the following 9-state model:

$$x_k^{TDDD} = [\Delta r_{x,k} \quad \Delta r_{y,k} \quad \Delta r_{z,k} \ \Delta v_{x,k} \quad \Delta v_{y,k} \quad \Delta v_{z,k} \ \Delta a_{x,k} \quad \Delta a_{y,k} \quad \Delta a_{z,k}]^T \tag{12}$$

The state transition matrix Φ_k^{TDDD} is determined as follows:

$$\Phi_k^{TDDD} = \begin{bmatrix} I_3 & t \cdot I_3 & t^2 \cdot I_3/2 \\ 0_3 & I_3 & t \cdot I_3 \\ 0_3 & 0_3 & I_3 \end{bmatrix} \tag{13}$$

Where: $\Delta r_{i,k}$ is the receiver position error in the ECEF system; $\Delta v_{i,k}$: is the receiver velocity error in the ECEF system; $\Delta a_{i,k}$ is the receiver acceleration error in the ECEF system, i=x,y,z; I_3 is the identity matrix; t is the Kalman filter update interval.

Carrier phase measurement are expressed by

$$\lambda\Phi = \rho + c\delta t_s - c\delta t_u + \lambda N + \delta d_{eph} - \delta d_{iono} + \delta d_{tropo} + \eta \tag{14}$$

Where λ is the wavelength of the signal transmitted from the satellite, Φ is the measured carrier phase expressed in cycles; ρ is the satellite-receiver geometric distance (range); c is the speed of light; δt_s is the satellite clock bias; δt_u is the receiver clock bias; N is the integer ambiguity; δd_{eph} is the ephemeris error; $d_{iono}, \delta d_{tropo}$ are the ionospheric and tropospheric errors; and η represents other errors. The parameters with indices s and u correspond to the satellite and the receiver, respectively.

Determine the difference between two consecutive carrier phase measurements at two epochs k+1 and k, as follows:

$$\begin{aligned} \lambda\Phi_{k+1} &= \lambda\Phi_{k+1} - \lambda\Phi_k \\ &= \rho_{k+1} - \rho_k + c\Delta\delta t_s - c\Delta\delta t_u + \delta\Delta d_{eph} \\ &- \Delta\delta d_{iono} + \Delta\delta d_{tropo} + \Delta\eta \end{aligned} \tag{15}$$

Since the components $c\Delta\delta t_s, \Delta\delta d_{iono}, \Delta\delta d_{tropo}, \delta\Delta d_{eph}$ exhibit negligible change over time, they are considered zero, and the equation (15) becomes:

$$\lambda\Phi_{k+1} = \rho_{k+1} - \rho_k - c\Delta\delta t_u + \varepsilon \tag{16}$$

Where ε represents the other errors. Equation (16) is rewritten as follows:

$$\lambda\Phi_{k+1} = e_{k+1}\left[r_{s,k+1} - r_{u,k+1}\right] - e_k\left[r_{s,k} - r_{u,k}\right] - c\Delta\delta t_u + \varepsilon \tag{17}$$

The receiver position at time $k+1$ is predicted from the estimated position value at step k as follows

$$r_{u,k+1} = \hat{r}_{u,k} + \Delta r_{u,k} \tag{18}$$

The equation (17) then takes the following form:

$$\begin{aligned} \lambda\Phi_{k+1} = e_{k+1}\left[r_{s,k+1} - r_{u,k}\right] - e_k\left[r_{s,k} - \hat{r}_{u,k}\right] - e_{k+1}\Delta r_{u,k} \\ - c\Delta\delta t_u + \varepsilon \end{aligned} \tag{19}$$

$$\lambda\widetilde{\Phi}_{k+1} = \lambda\Phi_{k+1|k} - c\Delta\delta t_u - e(t_k)\Delta r_u + \varepsilon \tag{20}$$

Where e_k the line-of-sight vector from the satellite to the receiver, is determined as follows:

$$e_k = \frac{r_{s,k} - r_{u,k}}{norm(r_{s,k} - r_{u,k})} \tag{21}$$

$$\Phi_{k+1|k} = e_{k+1}\left[r_{s,k+1} - r_{u,k}\right] - e_k\left[r_{s,k} - \hat{r}_{u,k}\right];\ \widetilde{\Phi}_{k+1} = \lambda\Phi_{k+1} \tag{22}$$

Equation (22) can be expressed as:

$$\lambda\Delta\widetilde{\Phi} = \widetilde{\Phi}_{k+1} - \Phi_{k|k+1} = -e(t_k)\Delta r_u - c\Delta\delta t_u + \varepsilon \tag{23}$$

$\widetilde{\Phi}_{k+1}$: The measured carrier phase value, provided by the MULTI-CORRELATOR block;

$\Phi_{k+1|k}$: The predicted carrier phase value is determined in the NAVIGATION PREDICTION block.

Therefore, utilizing the carrier phase measurement directly provided by the MULTI-CORRELATOR block/module helps to eliminate errors caused by the ionosphere and ephemeris, as well as minimizing the impact of cycle-slips since there is no requirement to determine accumulated carrier phase values.

To eliminate the influence caused by the receiver clock bias, the carrier phase measurement is differenced between satellites i end j, yielding the Single-Difference carrier phase measurement z_{CP}^{ij} provided to the NAVIGATION FILTER as follows:

$$z_{CP}^{ij} = \lambda\Delta\widetilde{\Phi}^i - \lambda\Delta\widetilde{\Phi}^j = [e^j(t_k) - e^i(t_k)]\Delta r_u + \varepsilon\varepsilon \tag{24}$$

Therefore, utilizing the intersatellite carrier phase measurement helps to eliminate the error caused by the receiver clock bias. The corresponding measurement matrix H_{CP}^{ij} is determined as follows:

$$H_{CP}^{ij} = [e^j(t_k) - e^i(t_k), 0_{1x3}, 0_{1x3}] \tag{25}$$

Where 0_{1x3} is 1× 3 zero matrix, and $\varepsilon\varepsilon$ represents other error components.

The PRR measurement value at step k+1 is determined from the estimated Doppler frequency value identified by the signal tracking loop of satellite j at step k+1 as follows:

$$\widetilde{prr}_{k+1}^{j} = -\hat{f}_{k+1}\frac{c}{F_{carrier}} \tag{26}$$

Where $\widetilde{prr}_{k+1}^{j}$: is determined in the NAVIGATION MEASUREMENT block.

The PRR value is determined from the navigation information and clock drift as follows:

$$\begin{aligned} prr_{k+1}^{j} = e_{k+1}^{j}\big[C_e^I(t_{tr})\cdot\big(v_{s,k+1}^{j}(t_{tr}) + \Omega_{ie}^{e}r_{s,k+1}^{j}\big) \\ -\big(v_{u,k+1} + \Omega_{ie}^{e}(r_{u,k+1})\big)\big] + \Delta t_{d,k+1} \end{aligned} \tag{27}$$

Where: t_{tr}: Transmission time, $C_e^I(t_{tr})$: the rotation matrix caused by the Earth's rotation during the time t_{tr}, which is determined as follows [1]:

$$C_e^I(t_{tr}) = \begin{pmatrix} \cos(\Omega) & \sin(\Omega) & 0 \\ -\sin(\Omega) & \cos(\Omega) & 0 \\ 0 & 0 & 1 \end{pmatrix} \tag{28}$$

Ω: Earth rotation angle during the signal's time of flight; $v_{s\ k+1}^{j}, r_{s\ k+1}^{j}$: The position and velocity values of satellite j in the ECEF frame at epoch k+1; $v_{u,k+1}, r_{u,k+1}$: Receiver Position and Velocity Values in the ECEF System at the step k+1;

Ω_{ie}^{e}: Earth's Rotation Velocity

Reformulate $v_{u,k+1}, r_{u,k+1}$ as follows:

$$\begin{aligned} v_{u,k+1} &= \hat{v}_{u,k} + \Delta v_{u,k} \\ r_{u,k+1} &= \hat{r}_{u,k} + \Delta r_{u,k} \end{aligned} \tag{29}$$

Subsequently, equation (27) can be expressed as:

$$\begin{aligned} prr_{k}^{j} = e_{k+1}^{j}\big[C_e^I(t_{tr})\cdot\big(v_{s,k+1}^{j}(t_{tr}) + \Omega_{ie}^{e}r_{s,k+1}^{j}\big) \\ -\big(\hat{v}_{u,k} + \Delta v_{u,k} + \Omega_{ie}^{e}(\hat{r}_{u,k} + \Delta r_{u,k})\big)\big] + \Delta t_{d,k+1} \end{aligned} \tag{30}$$

The combination of (26) and (30) yields the following equation

$$\begin{aligned} -\hat{f}_{k+1}\frac{c}{F_{carrier}} = e_{k+1}^{j}\big[C_e^I(t_{tr})\cdot\big(v_{s,k+1}^{j}(t_{tr}) + \Omega_{ie}^{e}r_{s,k+1}^{j}\big) \\ -\big(\hat{v}_{u,k} + \Delta v_{u,k} + \Omega_{ie}^{e}(\hat{r}_{u,k} + \Delta r_{u,k})\big)\big] + \Delta t_{d,k+1} \end{aligned} \tag{31}$$

Given $\Omega_{ie}^{e}\Delta r_{u,k} \cong 0$, equation (31) can be rewritten as:

$$\begin{aligned} -\hat{f}_{k+1}\frac{c}{F_{carrier}} - e_{k+1}^{j}\big[C_e^I(t_{tr})\cdot\big(v_{s,k+1}^{j}(t_{tr}) + \Omega_{ie}^{e}r_{s,k+1}^{j}\big) \\ -\big(\hat{v}_{u,k} + \Omega_{ie}^{e}(\hat{r}_{u,k})\big)\big] = e^{j}(t_k)\Delta v_{u,k} + \Delta t_{d,k+1} \end{aligned} \tag{32}$$

Let $prr_{k+1|k}^{j} = e_{k+1}^{j}\big[C_e^I(t_{tr})\cdot\big(v_{s,k+1}^{j}(t_{tr}) + \Omega_{ie}^{e}r_{s,k+1}^{j}\big) - \big(\hat{v}_{u,k} + \Omega_{ie}^{e}(\hat{r}_{u,k})\big)\big]$, equation (32) can be rewritten as:

$$\widetilde{\Delta prr}_{k}^{j} = \widetilde{prr}_{k}^{j} - prr_{k-1|k}^{j} = e^{j}(t_k)\Delta v_{u,k} + \Delta t_{d,k+1} \tag{33}$$

Where $prr_{k+1|k}^{j}$ is the predicted value determined in the NAVIGATION PREDICT block.

Perform the PRR measurement between satellite j and satellite i to eliminate the receiver clock rate error $\Delta t_{d,k+1}$, yielding the single difference PRR measurement z_{prr}^{ij} provided to the NAVIGATION FILTER as follows:

$$z_{prr}^{ij} = \widetilde{\Delta prr}_{k}^{j} - prr_{k+1|k}^{j} = [e^{j}(t_k) - e^{i}(t_k)]\Delta v_{u,k} \tag{34}$$

The corresponding measurement matrix H_{PRR}^{ij} is determined as follows:

$$z_k = [\delta\tilde{\tau}_k \quad \delta\tilde{\phi}_k] \tag{35}$$

The PRRR measurement value at step k+1, which is determined from the Doppler rate identified by the signal tracking loop at step k, is calculated in the NAVIGATION MEASUREMENT block as follows:

$$\widetilde{prrr}_{k+1}^{j} = -\dot{\hat{f}}_{k+1}\frac{c}{F_{carrier}} \tag{36}$$

The PRRR measurement value at step k+1 can be determined from the navigation information at step k+1 as follows:

$$prrr_{k}^{j} = e_{k+1}^{j}a_{u,k+1} = e_{k+1}^{j}\big(\hat{a}_{u,k} + \Delta a_{u,k}\big) + \Delta t_{dr,k} \tag{37}$$

The equation is obtained from (36) and (37) as follows:

$$-\dot{\hat{f}}_{k+1}\frac{c}{F_{carrier}} = e_{k+1}^{j}\left(\hat{a}_{u,k} + \Delta a_{u,k}\right) + \Delta t_{dr,k}$$
$$-\dot{\hat{f}}_{k+1}\frac{c}{F_{carrier}} - e_{k+1}^{j}\hat{a}_{u,k} = e_{k+1}^{j}\Delta a_{u,k} + \Delta t_{dr,k} \quad (38)$$

Let $prrr_{k+1|k}^{j} = e_{k+1}^{j}\hat{a}_{u,k}$, then:

$$\widetilde{\Delta prrr}_{k}^{j} = \widetilde{prrr}_{k+1}^{j} - prrr_{k+1|k}^{j} = e_{k+1}^{j}\Delta a_{u,k} + \Delta t_{dr,k} \quad (39)$$

Where $prr_{k+1|k}^{j}$ is the predicted value determined in the NAVIGATION PREDICTION block. Perform the PRRR measurement between satellite j and satellite i, yielding the *PRRR* measurement z_{prr}^{ij} which is supplied to the NAVIGATION FILTER as follows:

$$z_{prrr,k}^{ij} = \widetilde{\Delta prr}_{k}^{j} - \widetilde{\Delta prr}_{k}^{i} = \left[e_{k+1}^{j} - e_{k+1}^{i}\right]\Delta a_{u,k} \quad (40)$$

The corresponding measurement matrix H_{PRRR}^{ij} is determined as follows:

$$H_{PRRR}^{ij} = [\,0_{1x3}, 0_{1x3}, e^{j}(t_k) - e^{i}(t_k)] \quad (41)$$

2.3 Implementation of the Sequential Kalman Filter

In order to ensure the capability of the GNSS receiver to operate realtime at a high sampling frequency, the implementation of signal processing algorithms must be optimized. In this paper, the goal is to implement the TDDD method using a SKF combined with the NIS method to eliminate satellites with abnormal observations. The SKF is a variation of the Kalman filter designed to process measurements sequentially instead of grouping all of them into one large matrix. This method is particularly useful in systems with a large number of measurements or where the number changes over time. SKF helps to reduce computational cost, avoids the need to invert large matrices, and increases flexibility when adding or removing abnormal measurements. For the TDDD implementation problem, instead of performing calculations for all satellites simultaneously, the SKF is used for sequential estimation, utilizing the measurement from each satellite individually. After the GNSS receiver has tracked a sufficient number of satellites, the TDDD method requires initializing the values for position, velocity, acceleration, and clock error components. This initialization is performed by a Weighted Least Squares (WLS) estimator, as specifically presented in [20]. Once initialized, the TDDD method is implemented as shown in Figure 2, specifically as follows:

Step 1. Initialization of position, velocity, acceleration, and clock error using WLS

Step 2. Prediction

$$x_{k|k+1}^{TDDD} = \Phi_{k}^{TDDD}x_{k}^{TDDD}$$
$$\mathrm{P}_{k|k+1}^{TDDD} = \Phi_{k}^{TDDD}\mathrm{P}_{k}^{TDDD}(\Phi_{k}^{TDDD})^{T} + Q_k \quad (42)$$

Step 3. Sequential update for each satellite

Consider satellite 1 always as the reference satellite

For j=2: N

Step 3.1 Determine the measurement matrix z_k^j from (24), (34), (40); H_k^j from (25), (35),(41)

$$z_k^j = \left[z_{CP}^{1j}; z_{PRR}^{1j}; z_{PRRR}^{1j}\right]$$
$$H_k^j = \left[H_{CP}^{1j}; H_{PRR}^{1j}; H_{PRRR}^{1j}\right] \quad (43)$$

Step 3.2 Calculate the innovation

$$v_k^j = z_k^j - H_k^j x_{k|k+1}^{TDDD} \quad (44)$$

Step 3.3 Determine the innovation covariance S_k^{1j}

$$S_k^j = H_k^j \mathrm{P}_{k|k+1}^{TDDD} {H_k^j}^T + R_k^j \quad (45)$$

Step 3.4 Calculate the NIS

$$NIS_k^j = {v_k^j}^T {S_k^j}^{-1} v_k^j \quad (46)$$

Compare NIS_k^j with the threshold χ, which is determined based on the Chi-square distribution assumption of NIS_k^j using the degrees of freedom and confidence level [19].

Step 3.5 The state update is valid when $NIS_k^j < \chi$

$$K_k^j = \mathrm{P}_{k|k+1}^{TDDD} {H_k^j}^T (S_k^j)^{-1}$$

$$\hat{x}_{k+1}^{TDDD} = x_{k|k+1}^{TDDD} + K_k^j v_k^j \tag{47}$$

$$P_{k+1}^{TDDD} = (I - K_k^j P_{k|k+1}^{TDDD})$$

End.

III RESULTS AND DISCUSSION

3.1 Simulation conditions

The simulation conditions were designed to evaluate the performance of the implemented algorithms on the VT-GNSS receiver, using the Skydel GSG-8 simulator [21] to generate GPS L1CA signals. The simulated trajectory followed the dynamic model illustrated in Figure 3. Maximum velocity reached up to 3500 m/s (approximately 10 Mach), maximum acceleration reached up to 5g. To evaluate the effectiveness of the proposed hot-start mechanism, a series of 10 experimental trials were conducted to measure the TTFF**.** To assess the positioning performance of the receiver, the Root Mean Square Error (RMSE) of the determined position and velocity errors was evaluated. To verify the operation of the VT-GNSS receiver under conditions of high maneuverability and low signal intensity, the standard signal power of the simulator was gradually reduced from -130dBm to the following levels: -133dBm, -135dBm, -138 dBm.

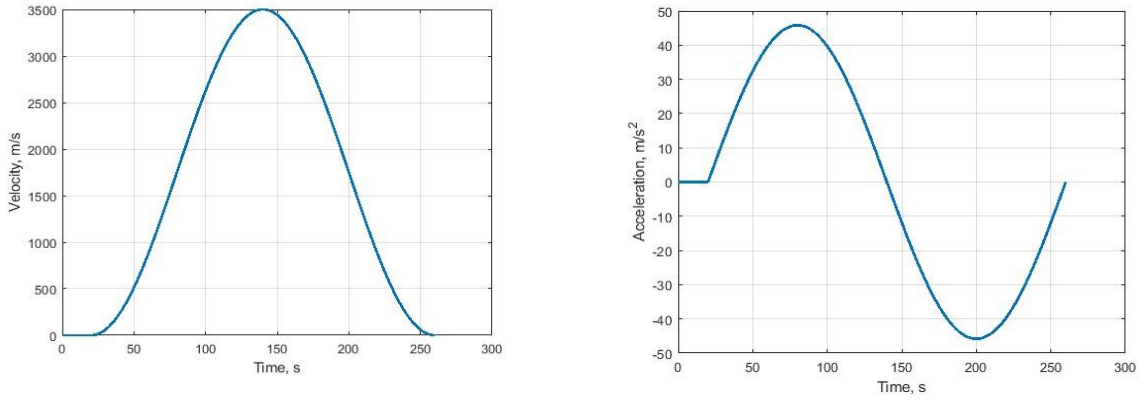

(a) (b)

Figure 3 Dynamic trajectory profile: (a) velocity profile; (b) acceleration profile.

3.2 Results

The experimental results for the Time To First Fix (TTFF) are summarized in Table 1

Table 1 TTFF, s

Trial No.	1	2	3	4	5	6	7	8	9	10
Hotstart	13.8	14.0	13.9	14.0	14.2	13.9	14.0	14.1	14.0	13.8
Coldstart	40.2	40.0	40.3	40.5	41.0	42.1	40.9	41.9	39.8	39.8

The empirical results demonstrate a significant performance improvement, with the TTFF being reduced from an average of 40 seconds (cold/warm start) to less than 15 seconds. This reduction confirms that the preflight injection of a priori position, time, and ephemeris effectively streamlines the signal acquisition process in the VT-GNSS receiver. The Figure 4 illustrates the Doppler frequency and Doppler rate values obtained by the VT-GNSS receiver when using NPF in the signal tracking loop, compared to the traditional approach using PLL. To verify the performance of the proposed model, the performance of the VT-GNSS receiver was compared across three cases: using NPF in the tracking loop and WLS in the navigation loop (NFP+WLS); using PLL in the tracking loop and TDDD in the navigation loop (PLL+TDDD); and using NPF in the tracking loop and TDDD in the navigation loop (NFP+TDDD).

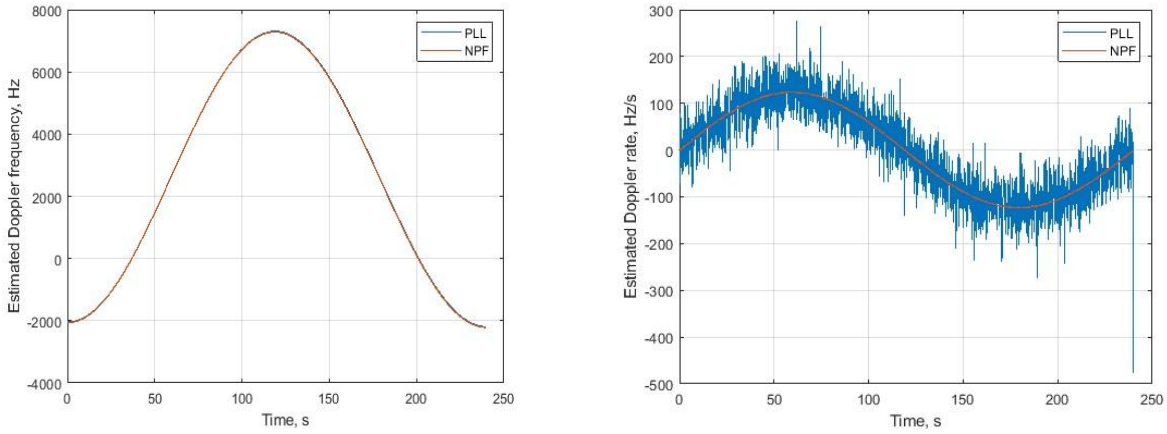

(**a**) (**b**)

Figure 4 Performance of the tracking loop: (a) comparative Doppler frequency; (b) Doppler rate.

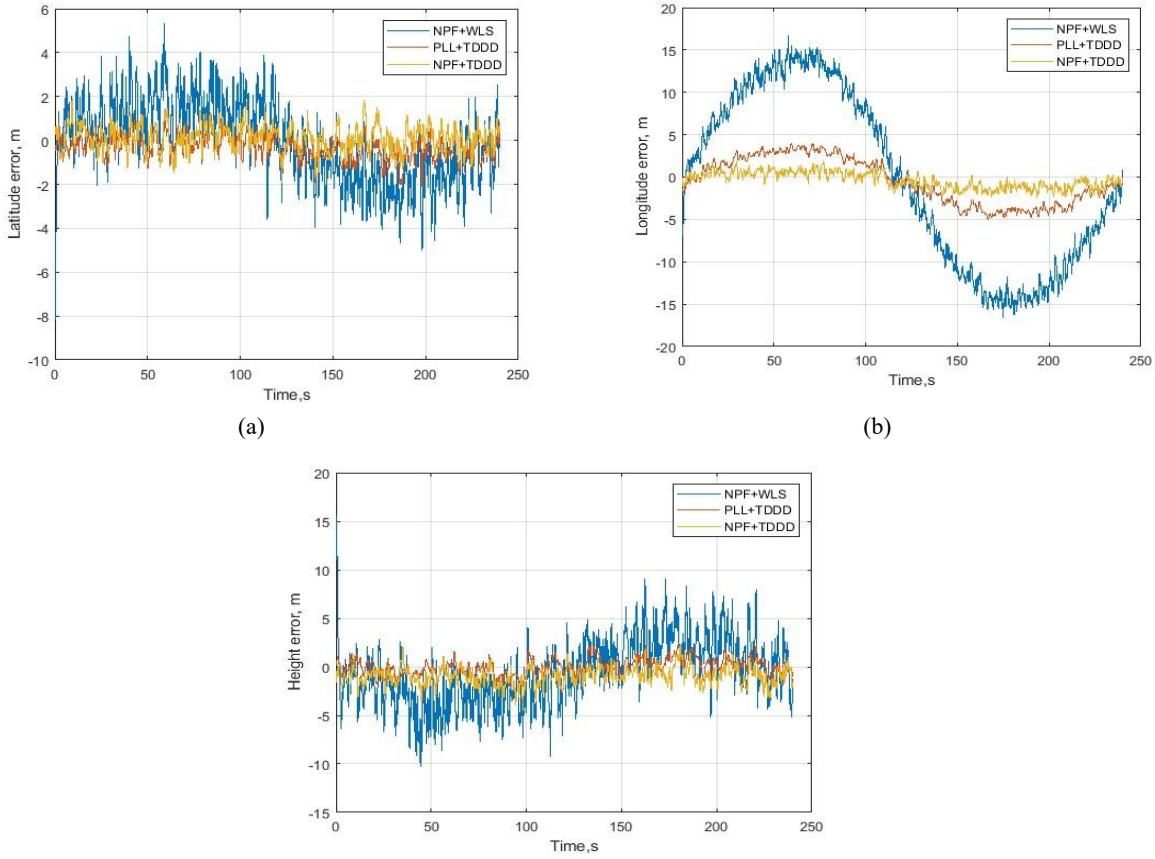

(a) (b)

(c)

Figure 5 Positioning Errors (m): (a) Latitude Error; (b) Longitude Error ; (c) Height Error

Table 2 Position RMSE.

Method	Latitude, RMSE,m	Longitude, RMSE,m
NPF+WLS	1.816	10.310
PLL+TDDD	0.633	2.772
NPF +TDDD	0.600	0.994

The Figure 5 illustrates the positioning error, while the Table 2 shows the RMSE values for the position errors in the three cases above.

The Figure 6 illustrates the velocity error, while the Table 3 shows the RMSE values for the velocity errors in the three cases above.

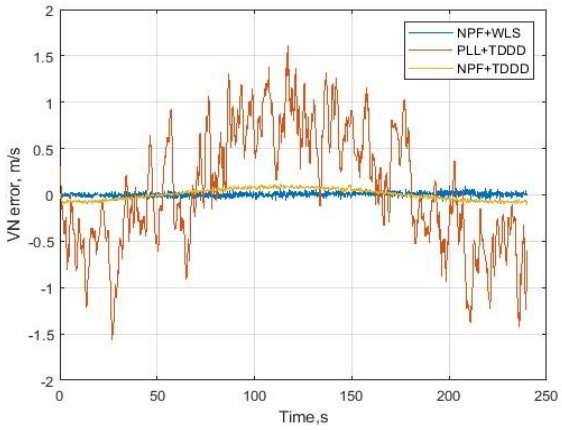

(a)

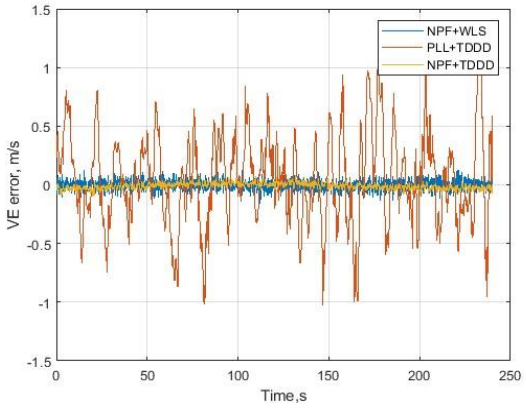

(b)

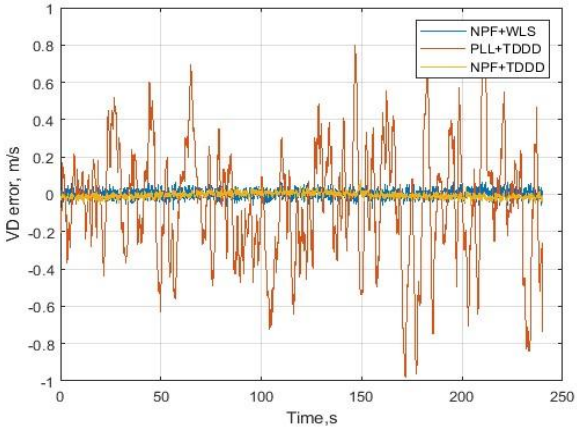

(c)

Figure 6 Velocity error components: (a) north velocity error V_N; (b) east velocity error V_E;(c) down velocity error V_D

Table 3 Velocity RMSE.

Method	V_N RMSE, m/s	V_E RMSE, m/s	V_D RMSE, m/s
NPF+WLS	0.022	0.042	0.023
PLL+TDDD	0.648	0.400	0.320
NPF +TDDD	0.059	0.027	0.016

The Figure 7 illustrates the estimated acceleration values and the acceleration estimation error over time.

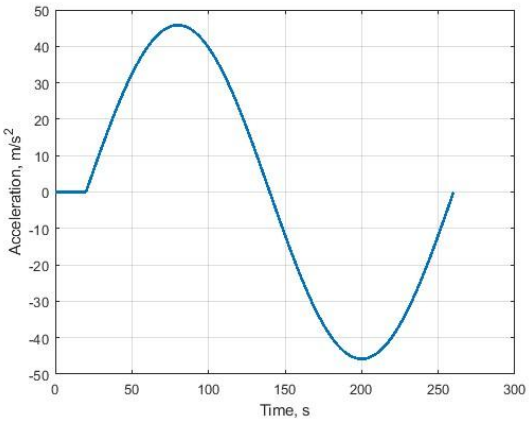

(**a**)

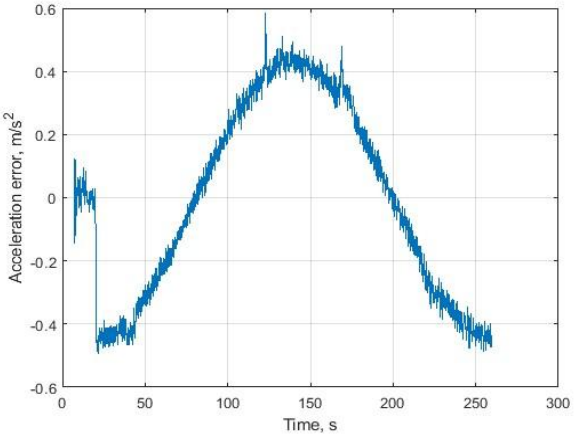

(**b**)

Figure 7 Acceleration estimation results: (a) estimated acceleration; (b) acceleration error

The proposed model demonstrated a significant enhancement in positioning and velocity performance when operating under high maneuver conditions compared to other standalone GNSS methods. Relative to the WLS method, the proposed architecture achieved substantial reductions in positioning errors: the longitude error was reduced by approximately 90.4%, while latitude and altitude errors were lowered by 67.0% and 62.1%, respectively. Furthermore, the model exhibited dramatically superior velocity estimation accuracy compared to a traditional PLL-based approach. The RMS velocity errors saw reductions of approximately 90.9% (north velocity), 93.3% (east velocity), and 95.0% (down velocity). These results unequivocally confirm the robustness and enhanced estimation capability of the proposed TDDD architecture in highly dynamic environments. Crucially, the system maintained a highly accurate estimation of acceleration, with errors consistently below 0.5 m/s^2.

The Figure 8 illustrates the position and velocity determination errors of the VT-GNSS receiver under the same trajectory but with successively reduced signal strength: -3dBm, -5dBm, -8dBm. The Table 4 presents the position RMSE values for the three cases above

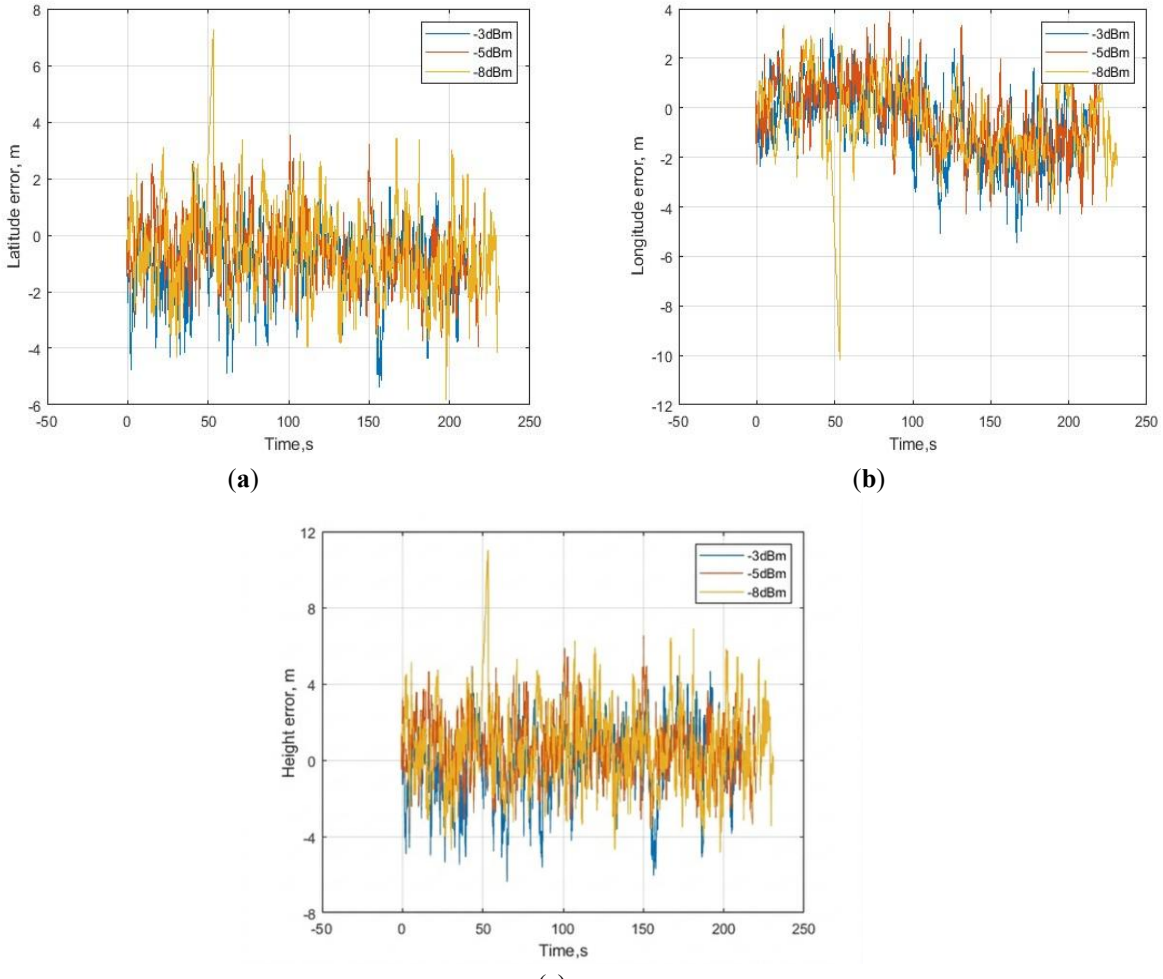

Figure 8 Positioning errors: (a) latitude error (m); (b) longitude error (m); (c) height error (m).

Table 4 Position RMSE.

Method	Latitude, RMSE,m	Longitude, RMSE,m	Height, RMSE (m)
-3 dBm	1.581	1.610	1.728
-5 dBm	1.322	1.438	1.391
-8 dBm	1.499	1.425	2.865

The Figure 9 illustrates the position and velocity determination errors of the VT-GNSS receiver under the same trajectory but with successively reduced signal strength: -3dBm, -5dBm, -8dBm. The Table 5 presents the position RMSE values for the three cases above

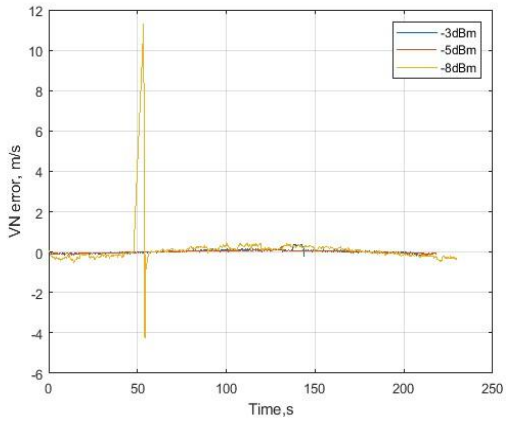

(a)

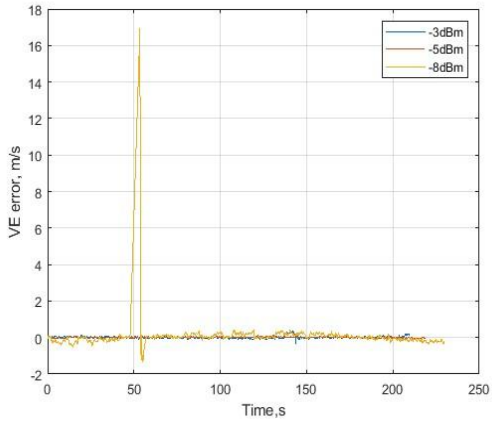

(b)

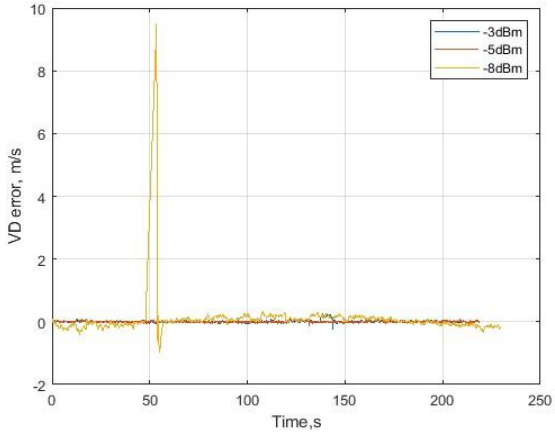

(c)

Figure 9 Velocity error components: (a) north velocity error V_N, m/s; (b) east velocity error V_E, m/s ; (c) down velocity error V_D, m/s.

Table 5 Velocity RMSE

Method	VN, RMSE, m/s	VE, RMSE, m/s	VD, RMSE, m/s
-3 dBm	0.088	0.059	0.040
-5 dBm	0.064	0.033	0.024
-8 dBm	0.307	0.395	0.266

3.3 Discussion

While the proposed NPF combined with the TDDD system achieved very low position and velocity errors, demonstrating superior stability under high maneuver conditions, there remains room for improvement in overall performance. Analysis of the results indicates that the acceleration estimation error is still significant, reaching approximately 0.5 m/s^2. This error primarily stems from complex higher order dynamics that are not fully modeled in the current state vector. To mitigate this impact on positioning and velocity accuracy, especially in extreme high dynamic scenarios, two main approaches can be considered for the TDDD Estimator's model. Firstly, the state model can be augmented by including higher order dynamic components (e.g., Jerk or Jounce) to more accurately estimate rapid acceleration variations. Secondly, applying techniques such as Adaptive Kalman Filtering [22] to dynamically adjust the process noise covariance matrix Q will provide a more robust and accurate estimation of these fast acceleration transients.

IV CONCLUSION

The proposed model demonstrated a significant improvement in positioning performance under high maneuver conditions compared to other standalone GNSS positioning methods. Specifically, relative to the method using WLS, our model achieved a reduction in longitude error of up to approximately 90.4 % while reducing latitude and altitude errors by approximately 67.0 % and 62.1%, respectively. Beyond positioning accuracy, the integrated hot-

start mechanism also yielded a substantial enhancement in temporal efficiency. Experimental trials confirmed that the TTFF was reduced by over 50%, dropping from an average of 40 seconds in cold-start mode to consistently under 15 seconds

This performance milestone is the result of the synergy between two key components: the 5-State NPF Tracking Loop, which utilizes a Kalman Filter to maintain a robust signal lock and provide reliable carrier phase measurements; and the 9-State TDDD Estimator, featuring an augmented model capable of estimating higher order acceleration components, thereby effectively suppressing dynamics related errors.

Furthermore, the system's deployment on the FPGA Zynq-7000 platform leverages the high speed, low latency, and parallel processing capabilities of its PS/PL architecture, ensuring the necessary accuracy and realtime operation. Regarding resilience to signal degradation, the proposed receiver maintained good performance even when signal intensity dropped sharply to 8dBm, keeping position errors (Latitude and Longitude) stable below 1.5 m. For velocity, the Sequential Kalman Filter exhibited adaptability and robustness as the velocity error only spiked briefly after sudden signal degradation and then converged to a stable value very rapidly, affirming the system's excellent dynamic stability.

V REFERENCES

[1] P. D. Groves, Principles of GNSS, Inertial, and Multisensor Integrated Navigation Systems, 2nd ed. Boston, MA, USA: Artech House, 2013.

[2] E. D. Kaplan and C. Hegarty, Understanding GPS/GNSS: Principles and Applications, 3rd ed. Norwood, MA, USA: Artech House, 2017.

[3] T. Pany, Navigation Signal Processing for GNSS Software Receivers, Boston, MA, USA: Artech House, 2010.

[4] Kim, J.; Kim, Y.; Song, J.; Kim, D.; Park, M.; Kee, C. Performance Improvement of Time-Differenced Carrier Phase Measurement-Based Integrated GPS/INS Considering Noise Correlation. Sensors 2019, 19, 3084. https://doi.org/10.3390/s19143084

[5] Zhang, T.; et al. GNSS Carrier Phase Improvement Using a MEMS INS by Integrating INS Dynamics into GNSS Tracking Loops. Navigation Study / Technical Report, 2024.

[6] Ren, J.; et al. Performance Analysis and Architectures for a MEMS-SINS/GPS Ultra-Tight Integration System with High Dynamic Performance.

[7] Yu, W.; Ding, X.; Dai, W.; Chen, W. Precise Point Positioning with Mixed Use of Time-Differenced and Undifferenced Carrier Phase Observations. J. Geod. 2018, 92, 135–152. https://doi.org/10.1007/s00190-017-1051-1

[8] Wang, H.; et al. Reliable Velocity Determination Through GNSS TDCP and Doppler Combination Using Factor Graph Optimization. Measurement 2025, 220, 115348. https://doi.org/10.1016/j.measurement.2024.115348

[9] Angrisano, A.; et al. Time-Differenced Carrier Phase Technique for Precise Velocity Estimation. Sensors 2022, 22, 9005. https://doi.org/10.3390/s22239005

[10] Guo, S.; Yang, H.; Gao, Y. Precise GNSS Positioning with Time-Differenced Carrier Phases at Variable Sampling Rates. Int. Arch. Photogramm. Remote Sens. Spatial Inf. Sci. 2025, XLVIII-G, 549–554. https://doi.org/10.5194/isprs-archives-XLVIII-G-2025-549-2025.

[11] Zhu, Z.; et al. Identification of Authentic GNSS Signals Using Time-Differenced Carrier Phase Measurements. Navigation 2025, 72(2), navi.698. https://doi.org/10.33012/navi.698

[12] Swamy, K.C.T. Time-Differenced Double Difference Method for Navigation with NavIC Receiver Differential Phase Bias. Measurement 2023, 215, 112625. https://doi.org/10.1016/j.measurement.2023.112625.

[13] Prochniewicz, D.; Kudrys, J.; Maciuk, M. Noises in Double-Differenced GNSS Observations. Energies 2022, 15, 1668. https://doi.org/10.3390/en15051668.

[14] Kettner, A. M.; Paolone, M. Sequential Discrete Kalman Filter for Real Time State Estimation in Power Distribution Systems: Theory and Implementation. IEEE Transactions on Instrumentation and Measurement 2017, 66, 2358–2370.

[15] Xilinx/AMD. Zynq-7000 All Programmable SoC Technical Reference Manual (UG585). 2023. Available online: https://docs.xilinx.com/v/u/en-US/ug585-Zynq-7000-TRM (Accessed on 27 November 2025).

[16] Hegarty, M.; O'Driscoll, A.; Petovello, M. Performance Evaluation of Advanced Tracking Loops for GNSS Receivers Operating in Challenging Environments. Remote Sens. 2017, 9, 298. https://doi.org/10.3390/rs9030298.

[17] O'Driscoll, C.; Lachapelle, G. Comparison of Traditional and Kalman Filter Based Tracking Architectures. In Proceedings of the European Navigation Conference, Naples, Italy, 3–6 May 2009; pp. 1–10

[18] Mu, R.; Long, T. Design and Implementation of Vector Tracking Loop for High-Dynamic GNSS Receiver. Sensors 2021, 21(16), 5629. https://doi.org/10.3390/s21165629.

[19] Gamse, S.; Nobakht Ersi, F.; Sharifi, M.A. Statistical Process Control of a Kalman Filter Model. Sensors 2014, 14, 18053–18076. https://doi.org/10.3390/s141018053

[20] Xu, J.; Zhang, S.; Cheng, X. A Real-Time Adaptive Weighted Least-Squares-Based Positioning Method for GNSS/INS Integration. Sensors 2023, 23, 580. https://doi.org/10.3390/s23010580.

[21] Orolia (Safran). Skydel GSG-8: Advanced GNSS Simulator. Available online: https://www.safran-navigation-timing.com/product/skydel-gsg-8-advanced-gnss-simulator (Accessed on 27 November 2025).

[22] Wang, D.; Chen, Q.; Jiang, K.; Zhao, J.; Du, X. A Robust Adaptive Extended Kalman Filter Based on an Improved Measurement Noise Covariance Matrix for the Monitoring and Isolation of Abnormal Disturbances in GNSS/INS Vehicle Navigation. Remote Sens. 2023, 15, 4125.